Biomechanics and Modeling in Mechanobiology (2019) 18:953–968
https://doi.org/10.1007/s10237-019-01123-7

ORIGINAL PAPER

The combined impact of tissue heterogeneity and fixed charge for models of cartilage: the one-dimensional biphasic swelling model revisited

Václav Klika[1,2] · Jonathan P. Whiteley[3] · Cameron P. Brown[4,5] · Eamonn A. Gaffney[2]

Received: 4 October 2018 / Accepted: 29 January 2019 / Published online: 6 February 2019

Abstract
Articular cartilage is a complex, anisotropic, stratified tissue with remarkable resilience and mechanical properties. It has been subject to extensive modelling as a multiphase medium, with many recent studies examining the impact of increasing detail in the representation of this tissue's fine scale structure. However, further investigation of simple models with minimal constitutive relations can nonetheless inform our understanding at the foundations of soft tissue simulation. Here, we focus on the impact of heterogeneity with regard to the volume fractions of solid and fluid within the cartilage. Once swelling pressure due to cartilage fixed charge is also present, we demonstrate that the multiphase modelling framework is substantially more complicated, and thus investigate this complexity, especially in the simple setting of a confined compression experiment. Our findings highlight the importance of locally, and thus heterogeneously, approaching pore compaction for load bearing in cartilage models, while emphasising that such effects can be represented by simple constitutive relations. In addition, simulation predictions are observed for the sensitivity of stress and displacement in the cartilage to variations in the initial state of the cartilage and thus the details of experimental protocol, once the tissue is heterogeneous. These findings are for the simplest models given only heterogeneity in volume fractions and swelling pressure, further emphasising that the complex behaviours associated with the interaction of volume fraction heterogeneity and swelling pressure are likely to persist for simulations of cartilage representations with more fine-grained structural detail of the tissue.

Keywords Cartilage modelling · Heterogeneity · Swelling pressure · Compaction

1 Introduction

Articular cartilage is found at the opposing ends of bones in joints and is thus subject to the extremes of physiological mechanics. In turn, cartilage is a complex biomaterial whose function is characterised by remarkable resilience and mechanical properties (Athanasiou et al. 2013). In particular, in conjunction with synovial fluid, cartilage maintains the separation of abutting joint bones, while supporting and spreading extreme loads, as high as 200 kg per square centimetre (Broom and Oloyede 1993; Hodge et al. 1986), and yet enables essentially friction-free relative motion of the joint bones over a lifetime of loading and unloading cycles.

Hence, a major driver in the mechanical study of cartilage tissue is the aim of elucidating how such extreme function emerges from cartilage structure. Furthermore, cartilage is prone to degeneration and pathology, driving an intense interest in the functional impact of degenerative processes within cartilage and whether artificial cartilage can be developed. As part of such investigations, numerous theoretical mechanical models for cartilage have been developed though most representations are built upon a core framework of a biphasic material with a solid phase, representing the cartilage collagen meshwork, and a fluid phase representing the

✉ Václav Klika
vaclav.klika@fjfi.cvut.cz

1 Department of Mathematics, FNSPE, Czech Technical University in Prague, Prague, Czech Republic

2 Present Address: Mathematical Institute, University of Oxford, Oxford, UK

3 Department of Computer Science, University of Oxford, Oxford, United Kingdom

4 Botnar Research Centre, NDORMS, University of Oxford, Oxford, UK

5 MERF, CPME, Queensland University of Technology, Brisbane, Australia

interstitial medium (Biot 1941; Mow et al. 1980, 1986). In addition, the impact of fixed charge attached to the collagen phase has regularly been incorporated from an early stage of model development due to its crucial role in cartilage behaviour (Lai et al. 1991; Huyghe and Janssen 1997; Gu et al. 1998; Wilson et al. 2005a). As reviewed in Ateshian (2007) and Klika et al. (2016), such models have recently been increasingly refined with the inclusion of ever more details such as heterogeneous distribution of solid matrix within cartilage, heterogeneous Darcy's law with preferential directions of flow determined by deformation, fibres, complex 3D geometries, and compaction effects that is the closing of fluid-filled pores (Wilson et al. 2005a, b, 2006; Ateshian 2007; Wilson et al. 2007; Chen et al. 2006; Ateshian et al. 2009; Pierce et al. 2013; Manzano et al. 2015, 2016).

Despite the undoubted benefit of having a more detailed description for cartilage tissue and hence the prospect of capturing its subtler behaviours in a wider context, there is also extensive merit in further developing our understanding of the fundamental properties associated with its core modelling framework. Such investigations can be directly applicable to relatively simple engineered soft tissue mimics (Murakami et al. 2015), as well as understanding aspects of more complex systems, in particular in appreciating and documenting the sensitivities and subtle behaviours that the foundations of soft tissue modelling propagate into feature-rich frameworks. For instance, the fundamental behaviour of the core model, albeit with heterogeneity, provides a baseline for understanding how mechanical responses broaden as increasing structural complexity is captured. Furthermore, such core models also provide an ideal platform to explore structural transitions in homeostasis, disease, and regeneration, which are essential for understanding musculoskeletal mechanics. Spatially, the structural transitions between or across tissues (Rossetti et al. 2017) are crucial to understanding physiological load carriage. Temporally, capturing low-level disease-related changes and feedback mechanisms (Brown et al. 2014) is of utility in exploring strongly coupled mechanical/biological processes such as osteoarthritis, especially in the context of understanding and optimising regenerative treatments. Such applications would require the representation of both spatial and temporal transitions between the relatively simple mechanics of a biomaterial (e.g. Raphael et al. 2017) with those of the more complex native tissue. Incorporating heterogeneity with the solid and fluid phases, together with fixed charge, our approach can thus ultimately provide a well-understood framework for representing normal, diseased, synthetic, or regenerating cartilage within the same core model while, importantly, including spatiotemporal transitions.

To proceed, we first rederive the core 1D biphasic model with fixed charged densities. This tracks the mechanics of the solid phase and its interspersed interstitial fluid phase, as well as the swelling pressure induced by fixed charges, which are assumed to be in quasi-equilibrium, a common and well-motivated simplifying assumption (Wilson et al. 2005a, b, 2006, 2007). In particular, such details are included as the derivation of cartilage models in the literature is not unified in the scaling of partial stress contributions with volume fractions and in the treatment of swelling pressure, which stands out especially once heterogeneity is present (Mow et al. 1980, 1986; Wilson et al. 2005a; Huyghe and Janssen 1997; Ateshian 2007; Klika et al. 2016). Hence, the presented model development first focuses on the appropriate inclusion of swelling pressure, not only at the cartilage–external bath interface, but also in the bulk, as detailed in Sect. 2.3. The model development then secondly focuses on a systematic consideration of initial and boundary conditions in Sect. 3.1, as these conditions are neither trivial nor follow from first principles and have only received detailed attention in relatively few studies (Hou et al. 1989; Ateshian 2007; Klika et al. 2016).

We subsequently proceed with our primary aim of documenting the behaviour of such core models in the simple setting of a one-dimensional confined compression experiment once material heterogeneity is present. However, in Sect. 3, we first demonstrate how the spatially homogeneous model's formulation can dramatically simplify for imposed velocity boundary conditions, where the solid displacement fully decouples from the pressure problem. This difference in model complexity, including boundary and initial conditions, as a result of spatial heterogeneity of the studied sample emphasises that heterogeneity in the presence of swelling pressure has an extensive impact even in the core framework of cartilage modelling. Hence, investigating this impact constitutes the overall aim and novelty of this study.

Consequently, we further explore the impact of heterogeneity through the use of numerical solutions of the governing equations, modelling one-dimensional confined compression testing, with a non-uniform initial distribution of volume fraction for the solid tissue phase and the interstitial fluid phase. In particular, our goal is to consider effects that are likely to be propagated into more complex models regardless of the choice of constitutive relation or model generalisation. Thus, we consider simple constitutive relations and simple, rotationally symmetric, confined compression testing. In such settings, our objective is to examine whether the details of laboratory testing, swelling pressure, and heterogeneity lead to sensitivities that quantitatively and substantively alter modelling predictions.

2 Cartilage as a biphasic electrically charged material

We proceed to develop the core biphasic representation of cartilage tissue, with a fluid and solid phase that are both incompressible and, between them, are space-filling with no voids. Firstly, let $\mathbf{X}$ denote Lagrangian coordinates for the solid phase, with V^s an arbitrary solid-phase Lagrangian volume. In contrast, let $\mathcal{V}^s(t)$, with $\mathcal{V}^s(0) = V^s$, denote the associated deformed, Eulerian, solid-phase volume, with $\mathbf{x}$ constituting Eulerian coordinates. The deformation gradient for the solid phase is thus given by $F_{iP} = \partial x_i/\partial X_P$, and as usual in single-phase continuum mechanics, the deformation gradient determinant, J, measures the volume change of an infinitesimal volume element. Hence

$$\int_{\mathcal{V}^s} f^s(\mathbf{x})\,\mathrm{d}v = \int_{V^s} J(\mathbf{X}) f^s(\mathbf{X})\,\mathrm{d}V.$$

2.1 Mass balance

We do not consider any sources or sinks of mass for either the solid or fluid phase of cartilage. Adopting summation convention for repeated Latin indices throughout the text, the mass balance equations are therefore

$$\frac{\partial \rho^\alpha}{\partial t} + \frac{\partial}{\partial x_i}\left(v_i^\alpha \rho^\alpha\right) = 0, \tag{1}$$

where t is time, with $\alpha \in \{f, s\}$ labelling the fluid(f) and solid(s) phase for both the mass density, ρ^α, and velocity field, $\mathbf{v}^\alpha$.

Noting that $\mathcal{V}^s(t)$ is moving with velocity $\mathbf{v}^s$ and the Reynolds transport theorem,

$$\begin{aligned} 0 &= \int_{\mathcal{V}^s(t)} \left[\frac{\partial \rho^s}{\partial t} + \frac{\partial}{\partial x_i}\left(v_i^s \rho^s\right)\right]\mathrm{d}v = \frac{\mathrm{d}}{\mathrm{d}t}\int_{\mathcal{V}^s(t)} \rho^s(\mathbf{x})\mathrm{d}v \\ &= \int_{V^s} \frac{\partial}{\partial t}(J(\mathbf{X})\rho^s(\mathbf{X}))\mathrm{d}V, \end{aligned}$$

the solid mass balance can now be rewritten in the local form

$$\frac{\partial}{\partial t}(J\rho^s) = 0. \tag{2}$$

It is convenient to express the balance laws using volume fractions φ^α, which are defined as the ratio of the volume of phase α in a sufficiently small neighbourhood of $\mathbf{x}$ at time t to the total volume of both phases in the same neighbourhood. Hence, we have the relation $\rho^\alpha = \varphi^\alpha \rho_T^\alpha$, where the true density ρ_T^α—mass of a phase per volume of that phase—does not change due to incompressibility. Note that the mixture, however, is compressible as the phase distribution may change through fluid being squeezed out of, or sucked into, a volume with a non-trivial solid phase (Klika et al. 2016). In addition, the space-filling requirement of the phases requires the constraint

$$\varphi^f + \varphi^s = 1, \tag{3}$$

so that the cartilage has no voids.

The solid mass balance (2) can be integrated in Lagrangian coordinates to yield the equivalent condition

$$J\varphi^s = \varphi_0^s, \tag{4}$$

where φ_0^s represents the initial volume fraction distribution of the solid phase. The fluid mass balance can be reexpressed by combining the local mass balances (1) with the space-filling condition (3) to yield the conservation of total volume balance

$$\frac{\partial}{\partial x_i}\left(v_i^f \varphi^f + v_i^s \varphi^s\right) = 0. \tag{5}$$

2.2 Momentum balance with no swelling pressure and constitutive relations

Thermal, inertial, and gravity effects are typically negligible in cartilage (Klika et al. 2016), so that momentum conservation for the whole tissue is given by $\nabla \cdot \boldsymbol{\sigma}^{\mathrm{tot}} = 0$, where $\boldsymbol{\sigma}^{\mathrm{tot}}$ is the total stress, which we assume can be decomposed into contributions from both phases in proportion to their volume fraction so that

$$\boldsymbol{\sigma}^{\mathrm{tot}} = \varphi^f \boldsymbol{\sigma}^f + \varphi^s \boldsymbol{\sigma}^s. \tag{6}$$

However the momentum balance for each phase needs to consider interphase momentum exchange. Noting Newton's third law, this is equal and opposite between the phases and is given by

$$\mathbf{q}^s = -\mathbf{q}^f = \varphi^s \varphi^f \gamma(\mathbf{v}^s - \mathbf{v}^f) + \Delta\mathbf{q},$$

where γ is a drag coefficient, which is only constrained by constitutive choice[1], except that $\gamma \geq 0$ is required by the Second Law via the Coleman–Noll procedure.

Note that we assume a proportionality of the contributions to the stress from the volume fraction of each phase, so that there is no stress contribution in the limit of one of the phases being absent given a constitutive choice of fixed drag. Furthermore, although this volume fraction scaling of the momentum exchange between phases is more generally appropriate for other constitutive choices, including the Kozeny–Carman relation defined below (MacMinn et al. 2016), we nonetheless deviate from many presentations in the literature in its use (Mow et al. 1980, 1986; Huyghe and Janssen 1997; Wilson et al. 2005b; Julkunen et al. 2013).

[1] Throughout the text, a constitutive relation is any relation that is necessary for model closure and that is constrained by the Coleman–Noll procedure to ensure compliance with the Second Law.

The contribution $\Delta\mathbf{q}$ is constrained via by the Coleman–Noll procedure for thermodynamic consistency (Gurtin et al. 2010), which demands no violation of the Second Law under *any* material deformation. One finds from the lengthy Coleman–Noll procedure that the most parsimonious form for $\Delta\mathbf{q}$ is given by (Klika et al. 2016)

$$\Delta\mathbf{q} = \mathfrak{p}\nabla\varphi^f = -\mathfrak{p}\nabla\varphi^s,$$

where $\mathfrak{p}$ has dimensions of pressure and is the Lagrange multiplier for the space-filling constraint, $\varphi^f + \varphi^s = 1$. Hence, the contributions from this term physically represent the interphase forces required to guarantee that entropy production (of the whole mixture) is nonnegative (Gurtin et al. 2010) for any deformation of the virtual cartilage due to work done by the pressure, $\mathfrak{p}$, induced by ensuring the space-filling constraint holds. A possible interpretation can be seen in the Cahn–Hilliard-like free energy, where this term is a form of interface penalisation. Lemon et al. (2006) offer a different argument: the gradient of volume fraction is interpreted as a measure of the force difference across the element's surface in the direction of increasing interfacial contact.

The Coleman–Noll procedure also reveals that the simplest thermodynamically compatible phase stresses consistent with Eq. (6) and zero total momentum exchange are of the form (Klika et al. 2016)

$$\varphi^s\boldsymbol{\sigma}^s = \varphi^s\left(-\mathfrak{p}\boldsymbol{I} + \widehat{\boldsymbol{\sigma}}^s\right), \quad \varphi^f\boldsymbol{\sigma}^f = \varphi^f\left(-\mathfrak{p}\boldsymbol{I} + \widehat{\boldsymbol{\sigma}}^f\right), \tag{7}$$

where the additional—effective—stresses $\widehat{\boldsymbol{\sigma}}^\alpha$, $\alpha \in \{f, s\}$, have been introduced. Note that $\mathfrak{p}$ has been defined as a Lagrange multiplier and hence need not represent the isotropic contribution to fluid stress. However, the $\mathfrak{p}$-dominated interstitial dynamics of cartilage often leads to the approximation that $\widehat{\boldsymbol{\sigma}}^f \approx \mathbf{0}$, with a neglect of the fluid deviatoric stress, which we assume below. Such assumptions can be further motivated by considering the physical scales within cartilage. In the supplementary material of Klika et al. (2016), the scale of pressure, and thus normal stress, within cartilage is estimated to be 10^5 Pa, while the fluid velocity scale is estimated to be of the order of 10^{-10} m/s. We can also take the viscosity of water to give a viscosity scale estimate of 10^{-3} Pa s. Then, the scale of the normal stress such as pressure and the scale of the deviatoric fluid stress, which is induced by viscosity, are similar only if there is significant spatial variation in the fluid velocity field on the scale of $(10^{-3} \times 10^{-10}/10^5)\,\mathrm{m} \sim 10^{-18}$ m. This is multiple orders below the continuum length scale and thus parity of these two physical effects is not feasible; instead, deviatoric fluid stress is negligible on the scales of the dominant physics.

There is much more choice and variation in the constitutive choice of the solid-phase deviatoric stress though the simplest is linear Hookean elasticity, which in the 1D simulations below collapses to the Cauchy stress tensor

$$\widehat{\sigma}^s = \mu^s(J-1), \tag{8}$$

noting that the first Piola–Kirchhoff stress tensor and the Cauchy stress tensor are equal in one dimension.

More generally, there is no uniqueness in the choice of constitutive relation, nor in the choice of the weighted sum of mixture quantities (Klika 2014); hence, careful comparison with experiments is required to fully justify and parameterise such freedom. However, as we shall see below, the qualitative results preceding the numerical section are of a general character and are not restricted in validity to the constitutive choices. For example, compaction occurs whenever swelling pressure has a singularity for vanishing pore size; the essential implications of heterogeneity on the choice of initial conditions and model are general and can be anticipated to apply even in higher dimensions.

With the constitutive relations specified as above, while working with the total momentum balance rather than the solid-phase momentum balance without loss of generality, we have that the final linear momentum balance equations are

$$0 = -\frac{\partial\mathfrak{p}}{\partial x_i} + \frac{\partial}{\partial x_j}\left(\varphi^s\widehat{\sigma}^s_{ij}\right) = \frac{\partial\sigma^{\mathrm{tot}}_{ij}}{\partial x_j}, \tag{9}$$

$$\begin{aligned} 0 &= -\varphi^f\frac{\partial\mathfrak{p}}{\partial x_i} - \varphi^s\varphi^f\gamma(v^f_i - v^s_i) \\ &= -\gamma\varphi^s\left[\frac{\kappa}{\mu}\frac{\partial\mathfrak{p}}{\partial x_i} + \varphi^f(v^f_i - v^s_i)\right], \end{aligned} \tag{10}$$

where μ is the fluid viscosity and $\kappa = \mu\varphi^f/(\gamma\varphi^s)$ is the cartilage permeability.

Note the similarities between the fluid momentum balance, Eq. (10), and the classical D'Arcy's law. In the former, gradients of the Lagrange multiplier for the no voids constraint, $\mathfrak{p}$, are balanced by velocity differences in contrast to the balance of pressure gradients and velocities in D'Arcy's law.

We assume below one of two constitutive choices for the permeability κ, or equivalently for the drag coefficient γ. The first is that permeability is a positive constant, $\kappa = \kappa_0$ and the second choice is the more realistic Kozeny–Carman relation (Kozeny 1927; Barabadi et al. 2009),

$$\kappa = \kappa_0\left(\frac{\varphi^s_0}{\varphi^s(t)}\right)^2\left(\frac{\varphi^f(t)}{\varphi^f_0}\right)^3, \tag{11}$$

where permeability decreases to zero in the limit that the solid occupies all space.

2.3 The inclusion of swelling pressure

Osmotic swelling pressure is a consequence of fixed charge on the aggrecans of the solid phase inducing electrical double layers (Buschmann and Grodzinsky 1995; Batchelor 2011) and has long been recognised to be important in cartilage tissue and is typically represented using the Donnan model (Lai et al. 1991; Huyghe and Janssen 1997; Gu et al. 1998; Wilson et al. 2005a). With the notation that a tilde denotes a volume-based concentration, the volumetric fixed charge density $\tilde{c}^F$ satisfies

$$\int_{\mathcal{V}^s(t)} \varphi^f \tilde{c}^F \,\mathrm{d}v = \int_{V^s} \varphi_0^f \tilde{c}_0^F \,\mathrm{d}V, \text{ and so } \varphi^f \tilde{c}^F J = \varphi_0^f \tilde{c}_0^F,$$

as it is advected with the solid phase. Noting $\varphi^f = 1 - \varphi^s = 1 - \varphi_0^s/J$, we therefore can express the fixed charge density, $\tilde{c}^F$, in terms of initial conditions and the solid-phase deformation:

$$\tilde{c}^F = \tilde{c}_0^F \frac{\varphi_0^f}{J\varphi^f} = \tilde{c}_0^F \frac{1-\varphi_0^s}{J-\varphi_0^s}. \tag{12}$$

With the approximation that the interstitial fluid away from Debye layers is a 1:1 electrolyte bath of dissolved NaCl, with total ion concentration of $\tilde{c}_b$ which is assumed fixed below, the Donnan swelling pressure is given by (Buschmann and Grodzinsky 1995)

$$p^{\text{swell}} = RT\left(\sqrt{(\tilde{c}^F)^2 + \tilde{c}_b^2} - \tilde{c}_b\right), \tag{13}$$

where RT is the product of the gas constant and absolute temperature. This swelling pressure induces an external force per unit volume of $-\nabla p^{\text{swell}}$ in the total momentum balance. Furthermore, consistent with the definition of total mixture stress (6), the contribution from this swelling external force is partitioned between the phases according to volume fraction and hence the momentum balances, Eqs. (9), (10), become, for $\varphi^s \neq 0$,

$$\begin{aligned} 0 &= -\frac{\partial \mathfrak{p}}{\partial x_i} - \frac{\partial}{\partial x_i}\left(p^{\text{swell}}\right) + \frac{\partial}{\partial x_j}\left(\varphi^s \widehat{\sigma}_{ij}^s\right) = \frac{\partial \sigma_{ij}^{\text{tot}}}{\partial x_j}, \\ 0 &= \frac{\kappa}{\mu}\left(\frac{\partial \mathfrak{p}}{\partial x_i} + \frac{1}{\varphi^f}\frac{\partial}{\partial x_i}\left(\varphi^f p^{\text{swell}}\right)\right) + \varphi^f (v_i^f - v_i^s). \end{aligned} \tag{14}$$

The presence of $\nabla\varphi^f$ in the momentum balance is not unequivocal in the literature, including our recent work (Klika et al. 2016), and hence, we briefly discuss it here. First, it is a direct consequence of considering swelling pressure as an external force, which follows the treatment of conservative electrical forces in the context of the electrochemical potential for mixture theories (de Groot and Mazur 1984). Note that inclusion of an external force is also thermodynamically consistent and does not affect the Coleman–Noll procedure implemented in deducing the biphasic model without swelling (e.g. Gurtin et al. 2010). Secondly, upscaling mixture theories to multiphasic and multiconstituent frameworks, while explicitly including the effect of quasi-electrostatics, have been shown to give rise to the $\nabla\varphi^f$ term within the momentum balance (Bennethum and Cushman 2002). Finally, triphasic theory (Lai et al. 1991), treating the cartilage tissue via mixture theory in higher detail with the explicit consideration of ion dynamics, leads to the conclusion that the swelling pressure is present in its full form within the expression for total stress and scaled by φ^f within the fluid stress. This is exactly in line with our reasoning above, where swelling pressure without any scaling appears in the total stress balance while scaled with volume fraction within the fluid stress balance.

2.4 Compaction of pores

The swelling pressure contribution p^{swell} generally becomes very large if the tissue is extensively compressed, which may be associated with the closing of pores, the closer proximity of fixed charges and φ^f tending to zero, which is also known as compaction. In particular, noting the form of (14), we observe that

$$\frac{p^{\text{swell}}}{\varphi^f}\frac{\partial}{\partial x_i}\varphi^f \tag{15}$$

will blow up as φ^f tends to zero, except for special choices of spatial variation. Hence, the inclusion of swelling pressure typically introduces large forces for small fluid volume fraction. Thus, the mechanics associated with compaction is anticipated to be generally exhibited by this framework without the need for complex solid constitutive laws and many further degrees of freedom (Pierce et al. 2013). The above compaction mechanics is present in the simple setting of one-dimensional confined compression, which thus provides a useful setting for our study.

3 One-dimensional models

Throughout the rest of this paper, we focus on modelling a confined compression experiment, whereby a piece of cartilage tissue with initial height h_0 on a stiff, impermeable surface is compressed via a porous plunger with the cross-sectional area of the cartilage prevented from expanding by a confining and impermeable solid structure. Hence, the movement is one-dimensional, though to allow plunger movement and tissue

compression the plunger must be porous so that interstitial fluid can leak out as the tissue is compressed.

Writing the momentum and mass balance equations in one spatial dimension, with the elimination $\varphi^f = 1 - \varphi^s$, we have

$$0 = \frac{\kappa}{\mu}\left[\frac{\partial}{\partial x}\left(\mathfrak{p} + p^{\text{swell}}\right) + p^{\text{swell}}\frac{\partial}{\partial x}(\ln(1-\varphi^s))\right] + (1-\varphi^s)(v^f - v^s), \tag{16a}$$

$$0 = \frac{\partial}{\partial x}\left(\varphi^s\hat{\sigma}^s - (\mathfrak{p} + p^{\text{swell}})\right), \tag{16b}$$

$$0 = \frac{\partial}{\partial x}\left(v^s + (1-\varphi^s)(v^f - v^s)\right). \tag{16c}$$

Noting the simplicity of Lagrangian coordinates for boundary conditions and numerical simulation, we rewrite the above in terms of the solid phase material coordinate X, using $\partial x/\partial X = J$ in conjunction with eliminating φ^s via $\varphi^s = \varphi^s_0/J$, to yield

$$\begin{aligned} 0 &= \frac{\kappa}{\mu}\frac{1}{J}\left[\frac{\partial}{\partial X}\left(\mathfrak{p} + p^{\text{swell}}\right) + p^{\text{swell}}\frac{\partial}{\partial X}\ln(1-\varphi^s_0/J)\right] \\ &\quad + (1-\varphi^s_0/J)(v^f - v^s), \\ \frac{\partial}{\partial X}&\left(\frac{\varphi^s_0}{J}\hat{\sigma}^s - (\mathfrak{p} + p^{\text{swell}})\right) = 0 = \frac{\partial}{\partial X}\left(v^s + (1-\varphi^s_0/J)(v^f - v^s)\right). \end{aligned} \tag{17}$$

These are supplemented by Eqs. (12), (13) for the fixed charge and swelling pressure and thus constitute three equations for v^f, x, p given appropriate initial and boundary conditions, noting that $v^s = \partial x/\partial t$, where t is time and $J = \partial x/\partial X$.

While we systematically address initial and boundary conditions below, the fact the cartilage is on a solid and impermeable base, without loss of generality at $X = 0$, entails that $v^f = v^s = 0$ for $X = 0$. Hence, the final equality above can be integrated to show that $v^s + (1-\varphi^s_0/J)(v^f - v^s) = 0$, allowing the elimination of v^f in Eq. (17), while the second inequality allows gradients of $\mathfrak{p} + p^{\text{swell}}$ to be eliminated in terms of gradients of $\varphi^s_0\hat{\sigma}^s/J$. Working with the displacement of the solid phase, $u(X,t) = x(X,t) - X$ rather than the Eulerian coordinate $x(X, t)$, one thus has a second-order, nonlinear parabolic equation for $u(X, t)$,

$$\frac{\partial u}{\partial t} = \frac{\kappa}{\mu}\frac{1}{J}\left[\frac{\partial}{\partial X}\left(\varphi^s_0 J^{-1}\hat{\sigma}^s(J)\right) + p^{\text{swell}}\frac{\partial}{\partial X}\ln(1-\varphi^s_0/J)\right], \tag{18}$$

where $J = 1 + \partial u/\partial X$.

3.1 Boundary conditions and the simplest initial conditions

Given the above parabolic equation possesses a time derivative of $u(X, t)$, an initial condition is required for the displacement of the solid phase, $u(X,t) = x(X,t) - X$. The simplest is zero strain, which is zero displacement,

$$u(X, t=0) = 0, \tag{19}$$

though this initial condition will be subject to further scrutiny below, especially when heterogeneity is present. Also required is a specification of the initial volume fractions consistent with the space-filling constraint and the initial fixed charge distribution:

$$\begin{aligned} \varphi^s_0(X) &= \varphi^s(X, t=0) = 1 - \varphi^f(X, t=0), \\ \tilde{c}^F_0(X) &= \tilde{c}^F(X, t=0), \end{aligned} \tag{20}$$

though $\tilde{c}^F_0(X)$ is taken to be a constant below in practice, using the value of Table 1.

Two boundary conditions are required for $u(X, t)$. The first is zero displacement at the bottom of the impermeable chamber, located at $X = 0$, and we have already imposed zero fluid phase velocity at this substrate. These conditions are summarised by:

$$u(X=0,t) = 0, \quad v^f(X=0,t) = 0. \tag{21}$$

At the top of the cartilage tissue, $X = h_0$, the solid phase displacement velocity v^s or the total stress may be imposed. The former is a kinematic boundary condition, also referred to as stress relaxation, and one typically prescribes a fixed velocity of a porous plunger in the compression experiment followed by a fixed displacement, so that

$$u(X = h_0, t) = \begin{cases} -V^P t & t \in [0, t_0] \\ -V^P t_0 & t \geq t_0 \end{cases}. \tag{22}$$

However, recovering the stresses associated with the response of the virtual cartilage to these kinematic conditions requires the calculation of the Lagrange multiplier, $\mathfrak{p}$, which in turn requires a specification of $\mathfrak{p}$ at one of the boundaries, which we address below in the consideration of the alternative, stress, boundary condition. The latter condition corresponds to a creep experiment where a known normal stress σ^* is applied at the plunger. Assuming that the gauge freedom for $\mathfrak{p}$ is chosen such that $\mathfrak{p}$ represents the isotropic stress of the fluid phase, a force balance at the interface yields

$$\sigma^* = F^R/A = \left[-(\mathfrak{p} + p^{\text{swell}}) + \varphi^s_0 J^{-1}\hat{\sigma}^s\right]\Big|_{X=h_0}. \tag{23}$$

Here, A is the cross-sectional area of the tissue and F^R is the total reaction force of the tissue, with the final equality given by the stress at the top of the cartilage, on neglecting the stresses associated with viscous drag within the plunger, as justified in "Appendices".

However, the right-hand side of Eq. (23) is, by the equations of motion via Eq. (17), an unknown constant. Hence, a further condition is required and this is usually that the fluid

is free draining. In the absence of swelling pressure, this requires that the pore pressure, which is the isotropic stress in the fluid on the microscale, is balanced by the external pressure on the fluid, p^{ext}, which is atmospheric pressure upon neglecting the typically small contribution of viscous drag in the plunger pores. This gives simply

$$\mathfrak{p}|_{X=h_0} = p^{\text{ext}}. \tag{24}$$

In addition, this fixes the gauge freedom in the Lagrange multiplier, $\mathfrak{p}$, so that it corresponds to the isotropic stress, in turn ensuring that Eq. (23) uses the appropriate gauge choice to generate the normal stress. The generalisation to the presence of swelling pressure is straightforward. With a swelling pressure, the pore pressure is modelled as possessing a discontinuity of p^{swell} at the interface with the plunger fluid. Thus, we still have $\mathfrak{p} = p^{\text{ext}}$, which in turn gives the required jump in isotropic stress at the interface. Hence, Eq. (24) still holds both as a free draining condition and for fixing the gauge in the evaluation of the normal stress more generally. Furthermore, when the external pressure is simply constant atmospheric pressure, it is commonplace to use the gauge freedom in the Lagrange multiplier $\mathfrak{p}$ to set the pressure origin to be atmospheric pressure, so that $p^{\text{ext}} = 0$, and all physical isotropic stress and pressure predictions are then relative to this origin. *This gauge choice is always implemented below, so that atmospheric pressure is zero by the choice of pressure origin.* Finally, note that without tissue heterogeneity and when interested only in final stationary state, it is also common to introduce swelling pressure solely via a jump condition at the boundary of the tissue (Lang et al. 2014), though we do not pursue this equivalent formalism for determining the homogeneous stationary state.

3.2 Model specification summary

Given the total ion concentration in the interstitial fluid, $\tilde{c}_b$, together with a constitutive relation for the permeability, κ, and for the solid-phase deviatoric stress $\hat{\sigma}^s$, the cartilage solid deformation, $u(X,t) = x(X,t) - X$ is given by Eq. (18), a nonlinear second-order parabolic partial differential equation. One also requires initial conditions, which are given by (20) for the volume fractions, with the initial fixed charge density, $\tilde{c}_0^F$, taking the constant value in Table 1. An initial condition is also required for the initial displacement such as, but not necessarily, Eq. (19). In addition, one of the two boundary conditions is given by Eq. (21). The second boundary condition may either be kinematic, as given by (22) with condition (24) required to fully specify $\mathfrak{p}$, or a stress condition given by Eqs. (23), (24). This allows a specification of both the solid displacement, u, and the Lagrange multiplier, $\mathfrak{p}$, with the solid phase velocity v^s given by $v^s = \partial u/\partial t$, the volume fractions given by $J = 1 + \partial u/\partial X$, $\varphi^s = \varphi_0^s/J = 1 - \varphi^f$, the fixed charge given by Eq. (12), the swelling pressure given by Eq. (13) and the interstitial fluid velocity, v^f, given by Eq. (17).

4 The effect of heterogeneity in 1D

We first of all note that there is no equilibrium configuration of the cartilage with both zero stress and strain given (i) residual stress is absent, so that there is no solid stress when $J = 1$, i.e. a constitutive relation is used such that $\hat{\sigma}^s = 0$ when $J = 1$, (ii) the presence of fixed charge, $\tilde{c}^F \neq 0$, so that $p^{\text{swell}} \neq 0$ by Eq. (13) and (iii) a heterogeneous volume fraction, so that φ_0^s is not constant. Then, the absence of a zero stress–zero strain equilibrium follows from by Eq. (18), which reveals that $\partial u/\partial t \neq 0$ under these conditions. This is the first indication that fixed charge and tissue heterogeneity combine to generate non-trivial mechanics and hence we first consider the model with homogeneous volume fractions for comparison.

4.1 Homogeneous case

If the fixed charge and volume fractions are initially homogeneous, then p^{swell} can be written as a function of J alone, using Eqs. (12), (13). Hence, there is a function $g(J)$ with $g(J=1) = 0$, which we motivate below, and such that

$$\begin{aligned} p^{\text{swell}} \frac{\partial}{\partial X} \ln(1 - \varphi_0^s J^{-1}) &= -p^{\text{swell}} \frac{\varphi_0^s}{J(J - \varphi_0^s)} \frac{\partial J}{\partial X} \\ &= \frac{\partial}{\partial X}\left(\varphi_0^s J^{-1} g(J)\right). \end{aligned}$$

In turn, one has the identity

$$\begin{aligned} &\frac{\partial}{\partial X}\left(\varphi_0^s J^{-1} \hat{\sigma}^s(J)\right) + p^{\text{swell}}(\varphi_0^s, J) \frac{\partial}{\partial X} \ln(1 - \varphi_0^s J^{-1}) \\ &\quad = \frac{\partial}{\partial X}\left(\varphi_0^s J^{-1} \hat{\sigma}_{sw}^s\right), \end{aligned} \tag{25}$$

with $\hat{\sigma}_{sw}^s = \hat{\sigma}^s + g(J)$, so that the swelling pressure may be incorporated into an effective solid-phase constitutive relation, with the constraint $g(J=1) = 0$ entailing that the undeformed state possesses no stress.

The inclusion of swelling pressure into the solid-phase constitutive law via $\hat{\sigma}^s \to \hat{\sigma}_{sw}^s$, while disregarding the explicit form of swelling pressure effect elsewhere in the model, also necessitates a shift of pressure

$$\mathfrak{p} \to p_{sw} = \mathfrak{p} + p^{\text{swell}} + \varphi_0^s J^{-1} g(J),$$

as can be seen from the fluid momentum balance in Eulerian coordinates, Eq. (16):

$$\varphi^f(v^f - v^s) = -\frac{\kappa}{\mu}\left[\frac{\partial}{\partial x}\left(\mathfrak{p} + p^{\text{swell}}\right) + p^{\text{swell}}\frac{\partial \ln(1-\varphi^s)}{\partial x}\right] = -\frac{\kappa}{\mu}\frac{\partial p_{sw}}{\partial x}.$$

With this redefinition of the Lagrange multiplier, which is also consistent with the Coleman–Noll procedure (Klika et al. 2016), the total stress is the same in both formalisms. In particular, when the swelling pressure is explicit, the Cauchy stress is given by

$$-(\mathfrak{p} + p^{\text{swell}}) + \varphi_0^s J^{-1}\widehat{\sigma}^s \tag{26}$$

and this expression is the same as

$$-p_{sw} + \varphi_0^s J^{-1}\widehat{\sigma}^s_{sw},$$

that is the total Cauchy stress expression when the swelling is accommodated via the solid stress and a redefinition of the Lagrange multiplier.

Thus either would yield the same deformation given kinematic conditions. However, the free draining condition, Eq. (24), is not equivalent. Hence, in general, the formalisms are not equivalent in their predictions for the stresses supported by each phase within the model or when modelling with given stress boundary conditions.

Thus, the above reasoning highlights that the neglect of explicit swelling pressure in the momentum balances, with the assumption that such effects are represented via a measured effective constitutive response of the tissue, is of limited validity, even given the assumption of homogeneity. In particular, such neglect of an explicit swelling pressure should be restricted to scenarios associated with kinematic boundary conditions and only for predictions of displacement, thus preventing a comparison with experimentally accessible reaction forces and stresses (DiSilvestro and Suh 2001). Nonetheless, such restrictions do not preclude informative studies as evidenced by the Mow and Mansour linear biphasic model, Eq. (32) in Mow and Mansour (1977), though the model derivation provided here is, however, very different.

Furthermore, once there is tissue heterogeneity, as is the case for articular cartilage (Athanasiou et al. 2013), there are even more extensive difficulties in the neglect of explicit swelling pressure in the momentum balances. In particular, the alternative of nominally incorporating swelling pressure within a constitutive relation for the solid stress introduces nonlinear and non-local contributions in the relation between stress and deformation, as highlighted in Appendix 2. As such, incorporating the swelling pressure into the constitutive relations imposes needless complexity in the constitutive relations, not only in terms of the practicalities of selecting and parameterising a constitutive relation from experimental observation, but also in the context of Occam's razor. Hence, below we proceed to consider simple constitutive relations in the heterogeneous case, while explicitly considering the swelling pressure, in the modelling of compression tests.

4.2 Compression testing modelling

We proceed to consider the constructed modelling framework in the context of an experimental confined compression test of bovine patellae cartilage by DiSilvestro and Suh (2001). In particular, this test consists of placing cartilage under two straining phases, the initial phase constituting a 10% pre-straining, followed by no plunger movement with concomitant stress relaxation, prior to a final 5% straining. When the final 5% strain is reached, the plunger is held fixed for sufficient time to allow the tissue to relax once more. Furthermore, the normalised reaction force $\bar{F}^R$, *defined as the ratio of the peak force during the 5% straining period divided by the final equilibrium force*, is of particular interest below as it is reported in these experiments and roughly in the range of 8–10 (DiSilvestro and Suh 2001).

With this experimental setting as motivation and noting the nonlinearity and consequent intractability of the bulk equations, we therefore consider simulations of the model, summarised in Section (3.2). The permeability is either constant or given by the Kozeny–Carman relation (11), while the solid constitutive relation is given by Eq. (8) with the initial fixed charge of Table 1. The swelling pressure is specified via Eqs. (12), (13) and the parameters are given by Table 1, with zero boundary velocity when the plunger is stationary and a velocity associated with a strain rate of $0.001\ \text{s}^{-1}$ during plunger motion (see Table 1), unless explicitly stated otherwise. In addition, given the focus on tissue heterogeneity, we consider an initial heterogeneous solid volume fraction given by

$$\varphi_0^s(X) = 0.30 - 0.15X/h_0, \tag{27}$$

where h_0 is the initial height of the cartilage sample.

4.2.1 Initial deformation and the equilibrium state

Finally, modelling this confined compression experiment requires careful consideration of the initial solid deformation due to heterogeneity and swelling. In particular, zero initial displacement is typically unphysical in the context of experimental protocols unless the tissue is homogeneous or there is an absence of swelling pressure. Noting an assumption that there is no applied force prior to the start of an experiment, we instead determine the initial displacement given by the steady solution of the cartilage bulk equations, with zero stress relative to atmospheric pressure at the top surface.

By considering the steady version of the model, Eq. (18), subject to the same parameters and constitutive relations of

Table 1 Model parameter values

$\kappa_0 = 6.9 \times 10^{-9}\,\text{mm}^2$, $h_0 = 1.28\,\text{mm}$, $\mu = 10^{-6}\text{MPa s}$, $\mu^s = 0.269\,\text{MPa}$,
$\tilde{c}_0^F = 2 \times 10^{-4}\text{mmol mm}^{-3}$, $\tilde{c}_b = 3 \times 10^{-4}\text{mmol mm}^{-3}$,
$RT = 2478\,\text{MPa mm}^3\,\text{mmol}^{-1}$, $V^P = -h_0 \times 10^{-3}\text{mm s}^{-1}$.

These are taken from DiSilvestro and Suh (2001), with a typical strain rate of 0.001s^{-1}. The product of the gas constant and temperature, RT, is required for the swelling pressure, Eq. (13) as are the bulk ion concentration, $\tilde{c}_b$ and the scale of the fixed charge $\tilde{c}_0^F$. Note that the above plunger velocity V^P corresponds to a strain rate of $0.001\ \text{s}^{-1}$ when imposed for kinematic boundary conditions

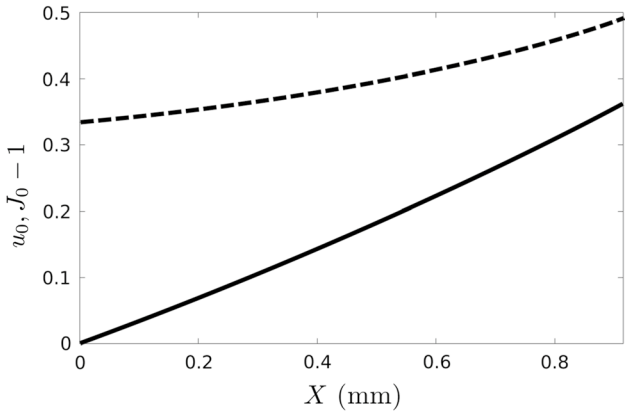

Fig. 1 The displacement, u_0 and swelling J_0 for the steady state associated with zero imposed stress. The steady state equations, (28), are solved with the parameters of Table 1, the solid volume fraction of Eq. (27) and zero stress conditions on the upper surface, which corresponds to h_0. The displacement, $u_0(X)$, due to the heterogeneity in the tissue is given by the solid line, and the dashed line plots $J_0(X) - 1$, where $J_0(X)$ is the steady Jacobian. Note that the initial displacement $u_0(X)$ is far from zero, as assumed in the zero strain initial conditions

the time dependent problem, together with the solid volume fraction of Eq. (27), we thus solve

$$0 = \frac{\partial}{\partial X}\left(\varphi_0^s(X) J_0^{-1} \widehat{\sigma}^s(J_0)\right) + p^{\text{swell}}(\varphi_0^s(X), J_0) \frac{\partial}{\partial X} \ln(1 - \varphi_0^s(X) J_0^{-1}) \tag{28}$$

for $u_0(X)$ with $J_0(X) = 1 + \partial u_0 / \partial X$. This is a second-order equation and thus requires two boundary conditions. However, it can be solved in a stepwise manner, initially as a first-order equation for J_0 with a stress-free boundary condition at the top of cartilage,

$$p^{\text{swell}}(J) - \varphi_0^s J^{-1} \widehat{\sigma}^s(J)\Big|_{X=h_0} = 0,$$

which follows from Eqs. (23), (24), with the pressure origin at atmospheric pressure, as detailed previously. The second step is then to integrate J_0 to obtain u_0 via the standard boundary condition, $u_0(X = 0) = 0$, corresponding to no displacement at the base of the sample.

The resulting profiles for associated $u_0(X)$ and $J_0(X)$ are plotted in Fig. 1. In particular, note that $u_0(X)$ is far from zero due to the presence of heterogeneity, and one might therefore expect very different predictions of tissue response using the steady state as an initial condition compared to the unphysical criteria of no bulk displacement. The steady state is used as the initial condition for displacement below unless stated otherwise, though prospective differences between the results using the two initial conditions constitute a core aspect of the subsequent computational investigations.

4.2.2 Computational results for compression testing

Sensitivity to stiffness, μ_0, permeability, κ_0 and plunger velocity, V_P.

We proceed to consider the time dependent problem of compression testing summarised in Sect. 3.2, with an initial reference set of parameters chosen according to the estimates and measurements presented in DiSilvestro and Suh (2001) and given in Table 1. As indicated by the illustrative results of Fig. 2, the simulations suggest that a constant permeability does not induce predictions of the normalised reaction force, $\bar{F}^R$, consistent with observation even when the elastic stiffness and permeability constant are varied over a range of two orders of magnitude around the reference parameters. This is further supported by simulations with additional parameter variations (not presented). In addition, Fig. 2 also demonstrates that the observed values of $\bar{F}^R \sim 8 - 10$ may be achieved once the permeability is given by the more realistic Kozeny–Carman constitutive relation, albeit for moderately different estimates of the tissue parameters. In particular, given the Kozeny–Carman permeability represents the effect of pore size reduction on permeability, this emphasises that capturing properties of the observed stress profile in compression testing requires the consideration in pore changes and material behaviour as compaction starts to occur.

This modelling observation is reinforced on considering when compaction is predicted to occur. To proceed, we denote the ratio of the parameter values with respect to their reference values listed in Table 1 with bars, i.e. $\bar{\mu}^s$, $\bar{\kappa}_0$ and this nomenclature is adopted throughout the results.

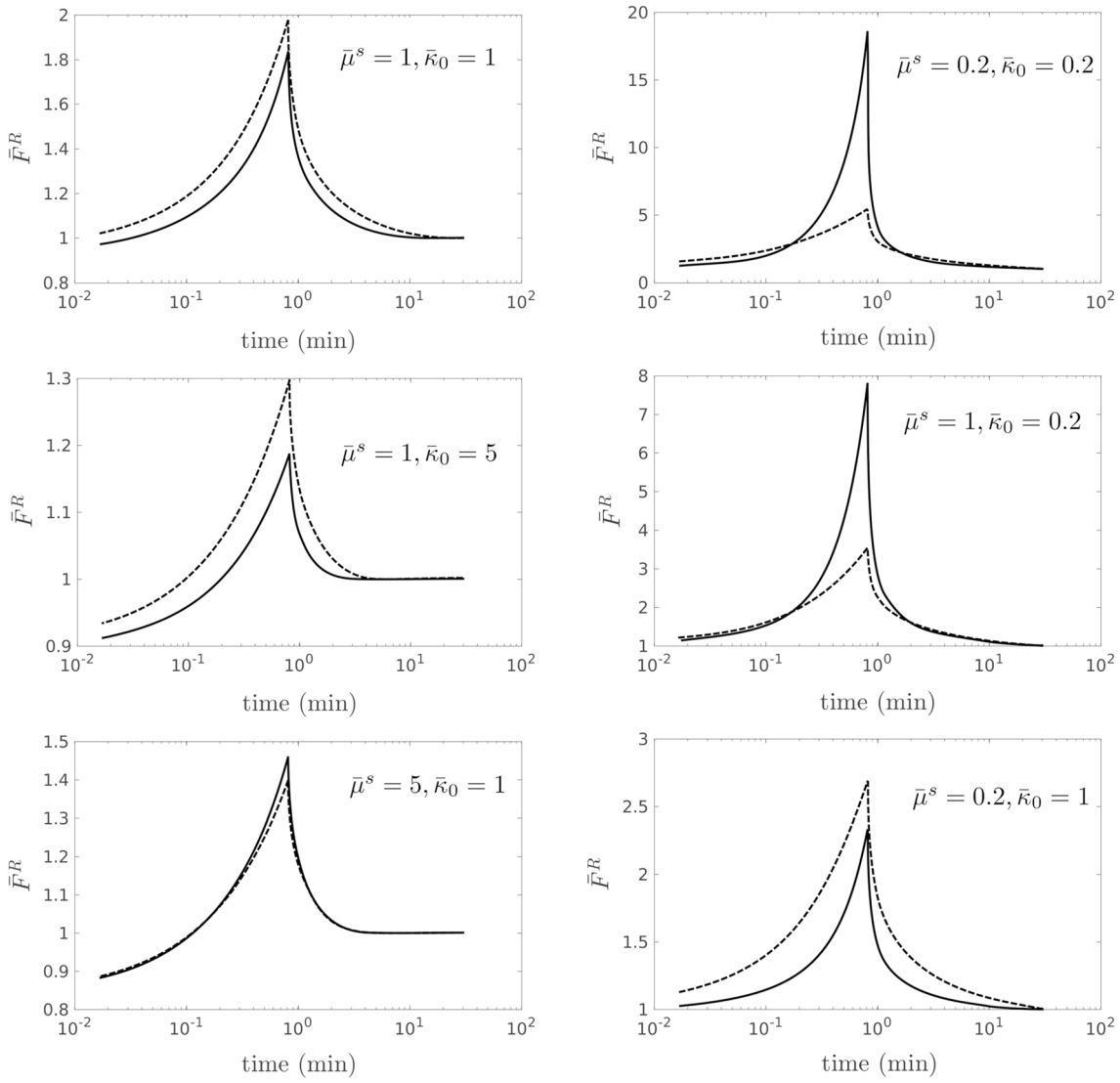

Fig. 2 The impact of changing the solid stiffness, μ^s and the tissue permeability, κ. The model is summarised in Sect. (3.2), with the solid constitutive relation of Eq. (8), the initial volume fraction of Eq. (27) and the parameters of Table 1, unless otherwise specified. Solid lines correspond to permeabilities given by the Kozeny–Carman relation, while dashed lines correspond to constant permeabilities. The initial conditions are associated with the heterogeneous solid volume fraction of Eq. (27), constant fixed charge, and the equilibrated state associated with zero stress on the upper surface. The modelled experimental conditions correspond to a pre-straining of 10%, followed a sufficient duration of no plunger motion to allow essentially complete tissue relaxation, followed by a subsequent 5% straining. Top, left. A reference simulation with the parameters of Table 1. Middle row, left. The reference simulation settings, as in the top left plot, except that κ_0 has been increased five times. Bottom, left. The reference simulation settings, except that the solid stiffness modulus, μ^s, has been increased five times. Top, right. The same simulation except that both the permeability, κ_0, and the solid stiffness parameter μ^s have been decreased five times. Middle row, right. The reference simulation settings, except that κ_0 has been decreased five times. Bottom, right. The reference simulation settings, except that the solid stiffness parameter, μ^s, has been decreased five times

Particularly, the predicted normalised reaction force, $\bar{F}^R$, of approximately 8 with $\bar{\mu}^s = 1$, $\bar{\kappa}_0 = 0.2$ and Kozeny–Carman permeability corresponds to a parameterisation that would yield compaction, i.e. the fluid volume fraction φ^f approaching zero, at a total, global, strain of 12.8% for the reference plunger velocity. In contrast, changing the stiffness and permeability parameters to $\bar{\mu}^s = 0.2$, $\bar{\kappa}_0 = 0.2$ results in $\bar{F}^R \sim 20$, though the plunger velocity in the pre-straining phase is halved to prevent this simulation stopping within the compression test due to a singularity of $\varphi^f = 0$ being reached. Furthermore, with these parameters for stiffness and permeability, together with the reference plunger velocity of Table 1, compaction occurs at a total strain of 9.6%. With this same adjustment in the plunger

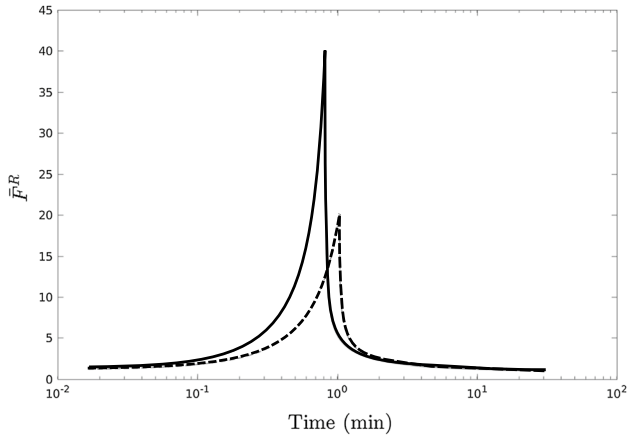

Fig. 3 Sensitivity to plunger velocity An illustration of the sensitivity of the peak normalised reaction force $\bar{F}^R$ to the plunger velocity V^P, with Kozeny–Carman permeability and $\bar{\mu}^s = 1$, $\bar{\kappa}_0 = 0.1$, with all other parameters and initial conditions as in Fig. 2 except for the plunger velocity, V_P. The plunger velocity in the pre-straining phase is half that of V^P listed in Table 1 to prevent the prospect of complete compaction, with $\varphi^f \to 0$, in the pre-straining period, noting the high normalised reaction forces. The prediction for the normalised reaction force with these choices is presented by the solid line, while the result associated with a decrease in plunger velocities by 20% is given by the dashed line, with an approximate halving of the predicted peak reaction force

velocity in simulating the compression test, further changing the parameters to $\bar{\mu}^s = 1$, $\bar{\kappa}_0 = 0.1$ yields $\bar{F}^R \sim 40$ with compaction at reference plunger velocities occurring at a total strain of 6.3%. Hence, higher normalised reaction forces can be induced, and higher effective stiffness occurs, in models of cartilage tissue that reach compaction under less strain.

The fact the force behaviour and loading capabilities of the medium has been altered by differing extents of compaction suggests the fluid drainage dynamics plays an important role in mechanical response, as further emphasised in Fig. 3, where differing normalised reaction forces are predicted for different forcing plunger velocities. Hence, the redistribution of fluid, as measured by volume fractions, is likely to be important and informative in the tissue response and is considered next, especially in the context of its heterogeneity.

Fluid redistribution, volume fraction heterogeneity and compaction

We further compare the draining behaviour in the two chosen constitutive relations for permeability. Hence, we compare simulations for the Kozeny–Carman relation for $\bar{\mu}^s = 1$, $\bar{\kappa}_0 = 0.1$ to simulations possessing constant permeability for $\bar{\mu}^s = 0.2$, $\bar{\kappa}_0 = 0.2$. Each of these choices corresponds to the highest values of the normalised reaction force for each constitutive relation in Fig. 2 and reveals a very distinct behaviour of fluid redistribution, as highlighted in Fig. 4.

In the case of constant permeability, a wave front in the solid volume fraction, φ^s, develops and subsequently moves through the tissue reaching significant depths, while the height of the wave front slowly increases. This allows overall compression strains of larger than 50%. However, with Kozeny–Carman permeability, the modelling results predict that an extensive draining of the top layers of cartilage takes place at sufficient pace to prevent replenishment via fluid from the deeper layers of cartilage. Eventually,

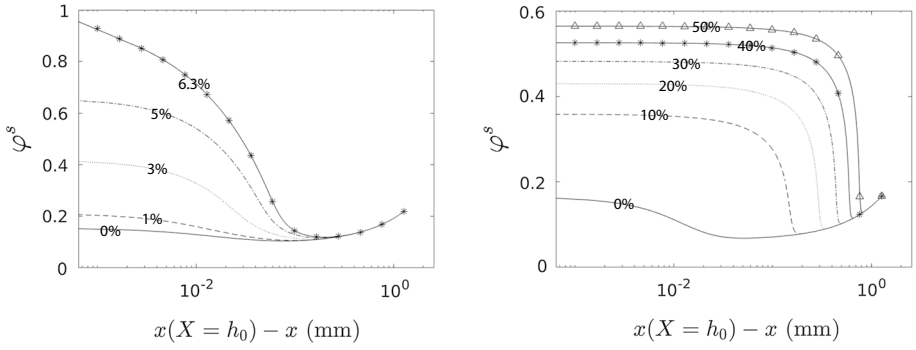

Fig. 4 The evolution of solid fractions with time in compression testing. All parameters are those of Table 1, except as specified. An illustration of how the solid volume fraction evolves in time for the Kozeny–Carman relation (*left*, $\bar{\mu}^s = 1, \bar{\kappa}_0 = 0.1$) and for constant permeability κ_0 (*right*, $\bar{\mu}^s = 1, \bar{\kappa}_0 = 0.1$). All other parameters and initial conditions are those of Fig. 2, except the plunger velocity in the initial pre-straining is halved on the left for Kozeny–Carman permeability, as in Fig. 3, to prevent the prospect of approaching complete compaction, where $\varphi^f = 0$. These plots highlight the fluid redistribution within the biphasic material. Curves demarcate different times in the evolution of the solid volume fraction, with each curve labelled by the total strain of the material in the simulation. Kozeny–Carman permeability (left) is predicted to approach complete draining, with $\varphi^f \to 0$, at the top layer of the cartilage. Constant permeability (right) in contrast is predicted to induce the formation of a solid volume fraction wave front that travels deep inside the tissue forcing global compression with more than 50% total strain. This distinction appears to be responsible for the difference of the peak normalised reaction force, where constant permeability yields $\bar{F}^R \approx 5$ while Kozeny–Carman relation gives $\bar{F}^R \approx 40$.

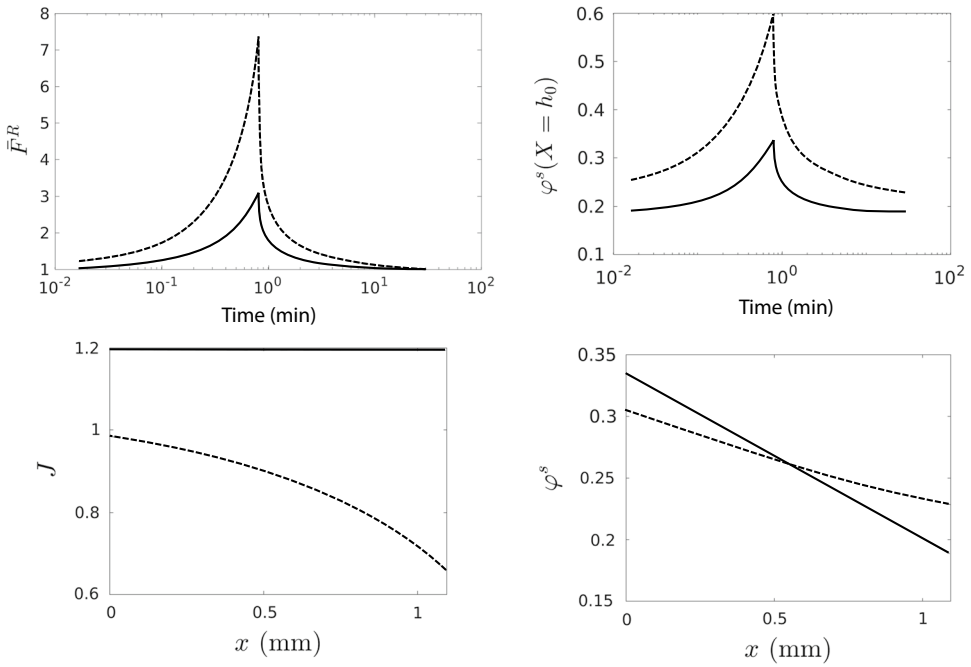

Fig. 5 The impact of initial conditions on the predicted applied stress and spatial heterogeneity. Simulations for the model summarised in Sect. 3.2, the parameters of Table 1, the solid constitutive relation of Eq. (8), Kozeny–Carman permeability and the initial volume fraction of Eq. (27). The modelled experimental conditions correspond to a pre-straining of 10%, followed by 30 minutes of relaxation and subsequently 5% straining. *Top left* The time evolution of the normalised reaction force $\bar{F}^R$ for an initial condition given by the equilibrium solution, $u_0(X)$, and thus implicitly assuming the model tissue has relaxed by the start of the experiment (shown as solid lines). The analogous predicted normalised reaction force when imposing an initial condition of zero displacement, $u(t = 0, X) = 0$, is depicted using dashed lines. Similarly, note the significant differences in the evolution of volume fraction at the top surface of the cartilage $X = h_0$, as well as the final profiles of the Jacobian and volume fractions for these two initial conditions

this leads to a compaction for as small strains as 6.3% for the parameters of Table 1, which differ from those of Fig. 4 as the latter has a slower initial plunger velocity. More generally, we have predictions of tissue response mechanics that are not only sensitive to the timescale associated with the strain rate of the plunger, but also possess a greater effective stiffness with heterogeneous drainage, localised to the top of cartilage, given Kozeny–Carman permeability. In turn, these modelling predictions highlight that gradients of volume fraction can facilitate the support of relatively large loads.

The impact of initial conditions

We compare model behaviour for two initial conditions, with first given by zero initial displacement and the second corresponding to the steady solution for displacement, as detailed in Sect. 4.2.1.

One may immediately observe that the internal mechanics is predicted to be different for these initial conditions as explored in Fig. 5. In particular, the temporal peak of normalised reaction force is 3.08 with the equilibrated initial conditions and 7.37 for the zero initial displacement in the modelled confined compression experiment. Analogously, major differences are observed for the volumes fractions within the tissue and the Jacobian. In turn, this emphasises that model selection and parameter estimation, based on comparing the model with experiment, will be sensitive to simulation initial conditions, simplifications such as assuming constant permeability and the details of the experimental protocol.

5 Discussion and conclusions

We have explored the impact of heterogeneity for modelling soft tissue via a biphasic swelling framework that incorporates both solid and interstitial fluid mechanics, together with the impact of fixed charges and the associated swelling pressures. Noting that there is no general consistency in model specification in the literature, especially with regard to gradients of the solid and interstitial fluid phases, a careful derivation of the resulting equations is given, including initial and boundary conditions. Given the emphasis on fundamental model behaviour and sensitivities, we have focused on simple constitutive relations and one-dimensional spatial dynamics, in particular confined compression tests.

The relative simplicity of homogeneous models

On relaxing heterogeneity, one finds a simple model that maps onto previous frameworks given kinematic boundary

conditions, as implicitly considered in classical observations of Lu and Mow for instance (Lu and Mow 2008). In addition, for homogeneous tissue, zero stress and zero displacement are consistent with the equilibrium state, entailing one can include the impact of swelling stresses implicitly into constitutive relation for solid in a relatively straightforward manner. However, one should note that even this case of a homogeneous biphasic swelling model is perhaps deceptively simple, and breaks down with the use of fixed stress conditions for instance.

Furthermore, the swelling pressure cannot be incorporated into a constitutive relation between stress and strain readily, or locally, when there is heterogeneity in a biphasic swelling model. While our main focus is heterogeneity in the volume fraction of the solid and interstitial fluid phases, such comments equally apply for heterogeneity in other aspects of the model, for example the fixed charge density. Thus, firstly, we observe that one should explicitly consider swelling pressure in modelling compression tests for soft tissue and engineering soft tissue mimics that possess heterogeneity and such qualitative observations are independent of the details of the constitutive relation. Furthermore, even the briefest inspection of Eq. (18) emphasises that it is the interplay of non-trivial swelling pressure and heterogeneity that leads to much more complicated model mechanics, due to the contribution $p^{\text{swell}}\partial[\ln(1-\varphi_0^s/J)]/\partial X$.

Pore compaction

A further aspect of the model is that even with simple constitutive relations, mechanical consequences of squeezing fluid out of the tissue and thus effective pore closing are evident in the simulations. In particular, there is a substantial and sensitive increase in the magnitude of the normalised reaction force associated with the cartilage response, though reduced permeability with fluid volume fraction, as with the Kozeny–Carman relation, is required for extensive effects that match observations. In contrast, constant permeability did not approach compaction and did not yield sufficiently high peak normalised reaction forces to match observation.

Furthermore, for Kozeny–Carman permeability, volume fraction gradients, drainage and the approach to compaction are localised to close to the plunger, as well as being accompanied by a very high effective stiffness. In turn, this highlights that large gradients in volume fraction can emerge during compression and can serve to enhance load bearing. More generally, our modelling results highlight that pore compaction mechanics may be captured by simple constitutive relations coupled with heterogeneity and swelling pressure. Furthermore, unless the constitutive relation is carefully formulated, such effects are not observed in simple models of homogeneous tissue, which in turn provides another example of how the model behaviour increases in complexity on considering both heterogeneity and swelling pressure.

Sensitivity to initial conditions and experimental protocol

We have also demonstrated a sensitivity in modelling predictions in regard to the choice of initial conditions when heterogeneity and swelling pressure are present, due to the fact the zero stress and strain state is not an equilibrium solution; under such circumstances, the initial conditions need to be chosen carefully so as to match experimental conditions. Despite such difficulties and the need to apply forces to maintain zero displacement in the presence of both tissue heterogeneity and fixed charge, we note that zero displacement is a common choice of initial condition for compression test modelling (DiSilvestro and Suh 2001). However, this is not equivalent to imposing zero stress before the plunger starts compressing the cartilage tissue. Hence, one has quantitatively different predictions for force-displacement curves with the choice of initial conditions, which in turn would generate substantially different predictions for the estimation of material parameters for instance.

Assumptions of the model and their discussion

We have formulated a general model,[2] which we later simplified to a one-dimensional version to acquire insight into model properties and to identify appropriate initial and boundary conditions. The assumptions that led to the full model are (i) a biphasic mixture consisting of incompressible phases with no voids; (ii) negligible thermal, inertial and gravity effects; (iii) a framework of Coleman–Noll constraints for constitutive relations; (iv) the neglect of the fluid deviatoric stress, which is pressure-dominated dynamics and (v) the treatment of swelling pressure as an external force, in line with the concept of the electrochemical potential in mixture theory. We also justified the neglect of stress associated with the viscous drag within the plunger in typical situations. Further, we applied this model to a rotationally symmetric problem of confined compression, which has allowed the simplification to one dimension. The qualitative properties of the full model have been discussed in a general setting. Furthermore, in the simplified one-dimensional case where we further explored the indications from qualitative analysis, we considered Donnan's theory for osmotic pressure and two forms of constitutive relations for permeability, constant permeability on one hand and the Kozeny–Carman formula on the other. In addition, a linear constitutive relation for the solid phase was chosen. Finally, the fixed charge density was assumed to be depth dependent, while the initial condition for the solid deformation in the modelling of experimental confined compression procedures was typically determined from the long-time asymptotic steady state of free swelling relaxation.

[2] Specified in Eqs. (3), (4) and (5) or (1), (7), (14), (13)

Summary

We have from the above discussions the main finding of this study, namely that the fixed charge swelling stresses combined with heterogeneity can have a substantial impact on the formulation, behaviour and complexity of multiphase models of soft tissue, such as cartilage, and its engineered analogues. Our findings also further demonstrate the sensitivity of simulation predictions to how experimental conditions are represented, especially with regard to initial conditions. In addition, heterogeneous pore squeezing mechanics enhancing the load bearing capabilities of the modelled tissue is observed to emerge with Kozeny–Carman permeability. Such findings in turn emphasise the importance of heterogeneity and the need for both careful model specification and the faithful in-silico mimicry of laboratory studies for quantitative objectives, such as the estimation of material parameters including permeability constitutive relations and initial, possibly heterogeneous, volume fractions and displacements. Finally, we note that these observations have emerged from parsimonious models for simple laboratory tests. Hence, such mechanical behaviours and sensitivities are anticipated to be inherited by simulations of more sophisticated laboratory settings, in vivo scenarios and modelling more realistic, nonlinear and anisotropic, material responses, as well as more sophisticated constitutive relations, all of which characterise many current research directions.

Acknowledgements V.K. is grateful for support from the International Mobility of Researchers—MSCA-IF in Czech Technical University grant CZ.02.2.69/0.0/0.0/17_050/0008025 funded by The Ministry of Education, Youth and Sports (MEYS) of the Czech Republic, as well as support from the Mathematical Institute at the University of Oxford.

Appendix 1: The reaction force, F^R

The reaction force experienced by the plunger is given by $F^R = F^C + F^P$ where F^C is the force at the cartilage/plunger interface and F^P is the drag force due to the fluid movement through plunger pores. Here, our objective to determine F^C and to show that F^P is negligible compared to F^C, so that $F^R \approx F^C$.

We consider F^C first: if the plunger, excluding its pores, has cross-sectional area A, which assumed to be the same as the tissue cross-sectional area, then the force at the top of cartilage tissue is given by

$$F^C = \left[-(p + p^{\text{swell}}) + \varphi_0^s J^{-1} \widehat{\sigma}^s\big|_{X=h_0}\right] A, \tag{29}$$

as follows from the expression for total stress in Eq. (17).

To consider F^P, we further assume the pore cross sections are identical and uniformly distributed within the plunger, with a circular radius a^{pore} and a length equal to the plunger height, h^P, with $h^P \gg a^{\text{pore}}$. Given flow entry length scales in a pore are of the order of a^{pore} in inertialess flows (Durst et al. 2005) and the timescale of transients, $t \sim (a^{\text{pore}})^2 \rho/\mu \sim 10^{-7}$s (Grodzinsky 2000, Ch4.3), is ultrafast, we have fully developed Poiseuille flow in the pores. Hence, the flux through a single pore is (Grodzinsky 2000)

$$Q^P_{\text{pore}} = \frac{\pi (a^{\text{pore}})^4 \Delta p^P}{8 \mu h^P}, \tag{30}$$

where μ is the fluid viscosity and Δp^P is the unknown pressure drop across the plunger. Relating the plunger porosity, φ^P, to the number of pores, n_{pores}, via $\varphi^P = n_{\text{pores}} \pi (a^{\text{pore}})^2 / A$, the total flux through the plunger is

$$Q^P = Q^P_{\text{pore}} n_{\text{pores}} = \varphi^P \frac{(a^{\text{pore}})^2 A \Delta p^P}{8 \mu h^P}. \tag{31}$$

This is balanced by the flux of the fluid due to the plunger movement, $Q^P = A V^P$. Eliminating Q^P gives the pressure drop across the plunger in terms of V^P,

$$\Delta p^P = \frac{8 \mu h^P}{(a^{\text{pore}})^2 \varphi^P} V^P,$$

and for typical values, taken from Soltz and Ateshian (1998) and our estimate of $\varphi^P = 0.1$[3], one finds

$$\frac{\Delta p^P}{[\text{Pa}]} = 50 \frac{h^P}{[\text{mm}]}.$$

Unless the plunger porosity is unrealistically extreme, such pressures are negligible compared to typical stresses, which can reach as high as 100kPa; hence $F^P = A \Delta p^P$ is negligible and the reaction force is given by

$$F^R \approx F^C = \left[-(p + p^{\text{swell}}) + \varphi_0^s J^{-1} \widehat{\sigma}^s\big|_{X=h_0}\right] A. \tag{32}$$

Appendix 2: Constitutive equation heterogeneity

Our objective in this appendix is to highlight the complexity of the prospective constitutive relation in the presence of heterogeneity if the swelling pressure is not to be explicitly considered, but instead incorporated into an effective

[3] We can estimate the plunger porosity by considering the proportion of plunger radius corresponding to pores across the plunger diameter, $\sim (a/a_P) \times (4 n_{\text{pores}}/\pi)^{1/2}$, which reduce to $(4\varphi^P/\pi)^{1/2}$. Hence, $\varphi^P = 1/2$ would require 80% of the plunger radius to correspond to pores (e.g. $40\mu m$ pores separated by only $10\mu m$). On the other hand for $\varphi^P = 0.1$ we have a reasonable result that about one third of the plunger radius corresponds to pores, i.e. pores are separated by about double their diameter.

relation between stress and deformation. In particular, the solid effective stress, $\widehat{\sigma}^s_{sw}$, would be defined via

$$\frac{\partial}{\partial X}\left(\varphi_0^s J^{-1}\widehat{\sigma}^s_{sw}(X,J)\right)\overset{\text{def}}{=}\frac{\partial}{\partial X}\left(\varphi_0^s J^{-1}\widehat{\sigma}^s(X,J)\right) + p^{\text{swell}}(\varphi_0^s,J)\frac{\partial}{\partial X}\ln(1-\varphi_0^s J^{-1}).$$

Hence, noting both J and φ_0^s are functions of X, we have

$$\widehat{\sigma}^s_{sw}(X,J)-\widehat{\sigma}^s(X,J) = -\frac{J}{\varphi_0^s}\int_X^{h_0} \mathrm{d}\bar{X} p^{\text{swell}}(\varphi_0^s,J)\frac{\partial}{\partial \bar{X}}\ln(1-\varphi_0^s J^{-1}) + \widehat{\sigma}^s_{sw}(h_0,J(h_0))-\widehat{\sigma}^s(h_0,J(h_0)),$$

where $\bar{X}$ is a dummy integration variable. Given the presence of heterogeneity in deformation, fixed charge, or initial volume fractions, so that swelling pressure gradients are present and the swelling pressure does not behave trivially in the above integral, this constitutive relation is then very complex. In particular, the relation depends not only locally on the deformation, but also non-locally on the osmotic swelling pressure, tissue deformation and volume fraction distributions. Working with such complexity, rather than an explicit consideration of the swelling pressure, would be much more difficult in terms of the selection and parameterisation of a constitutive relation from experimental observations, as measurements throughout the tissue are required to determine the constitutive relation at any point. While non-local constitutive relations are not excluded on any fundamental physical grounds (at least if consistent with the Second Law), the alternative of considering the swelling pressure explicitly in the momentum balances governing cartilage mechanics is much simpler and thus preferable on the grounds of Occam's razor as well as practicality.

References

Ateshian G (2007) On the theory of reactive mixtures for modeling biological growth. Biomech Model Mechanobiol 6(6):423–445

Ateshian G, Rajan V, Chahine N, Canal C, Hung C (2009) Modeling the matrix of articular cartilage using a continuous fiber angular distribution predicts many observed phenomena. J Biomech Eng 131(6):061,003

Athanasiou K, Darling E, Hu J, DuRaine G, Reddi A (2013) Articular Cartilage. CRC Press, Boca Raton

Barabadi B, Nathan R, Jen KP, Wu Q (2009) On the characterization of lifting forces during the rapid compaction of deformable porous media. J Heat Transf Trans ASME 131(10):101006

Batchelor GK (2011) Field, forces and flows in biological systems. Cambridge University Press, Cambridge

Bennethum LS, Cushman JH (2002) Multicomponent, multiphase thermodynamics of swelling porous media with electroquasistatics: II. Constitutive theory. Transp Porous Media 47(3):337–362

Biot M (1941) General theory of three-dimensional consolidation. J Appl Phys 12(2):155–164

Broom N, Oloyede A (1993) Experimental-determination of the subchondral stress-reducing role of articular-cartilage under static and dynamic compression. Clin Biomech 8(2):102–108

Brown CP, Houle MA, Popov K, Nicklaus M, Couture CA, Laliberté M, Brabec T, Ruediger A, Carr AJ, Price AJ et al (2014) Imaging and modeling collagen architecture from the nano to micro scale. Biomed Opt Express 5(1):233–243

Buschmann M, Grodzinsky A (1995) A molecular model of proteoglycan-associated electrostatic forces in cartilage mechanics. J Biomech Eng 117(2):179–92

Chen Y, Chen X, Hisada T (2006) Non-linear finite element analysis of mechanical electrochemical phenomena in hydrated soft tissues based on triphasic theory. Int J Numer Methods Eng 65(2):147–173

DiSilvestro MR, Suh JKF (2001) A cross-validation of the biphasic poroviscoelastic model of articular cartilage in unconfined compression, indentation, and confined compression. J Biomech 34(4):519–525

Durst F, Ray S, Unsal B, Bayoumi O (2005) The development lengths of laminar pipe and channel flows. ASME J Fluids Eng 127:1154–1160

Grodzinsky A (2000) An introduction to fluid dynamics. Garland Science, London

de Groot SR, Mazur P (1984) Non-equilibrium thermodynamics. Dover Publications, New York

Gu W, Lai W, Mow V (1998) A mixture theory for charged-hydrated soft tissues containing multi-electrolytes: passive transport and swelling behaviors. J Biomech Eng 120(2):169–180

Gurtin M, Fried E, Anand L (2010) The mechanics and thermodynamics of continua. Cambridge University Press, Cambridge

Hodge W, Fijan R, Carlson K, Burgess RG, Harris WH, Mann RW (1986) Contact pressures in the human hip joint measured in vivo. Proc Natl Acad Sci 83:2879–2883

Hou J, Holmes M, Lai W, Mow V (1989) Boundary conditions at the cartilage-synovial fluid interface for joint lubrication and theoretical verifications. J Biomech Eng 111(1):78–87

Huyghe J, Janssen J (1997) Quadriphasic mechanics of swelling incompressible porous media. Int J Eng Sci 35(8):793–802

Julkunen P, Wilson W, Isaksson H, Jurvelin J, Herzog W, Korhonen R (2013) A review of the combination of experimental measurements and fibril-reinforced modeling for investigation of articular cartilage and chondrocyte response to loading. Comput Math Methods Med. https://doi.org/10.1155/2013/326150

Klika V (2014) A guide through available mixture theories for applications. Crit Rev Solid State Mater Sci 39(2):154–174

Klika V, Gaffney EA, Chen YC, Brown CP (2016) An overview of multiphase cartilage mechanical modelling and its role in understanding function and pathology. J Mech Behav Biomed Mater 62:139–157

Kozeny J (1927) Ueber kapillare Leitung des Wassers im Boden. Sitzungsber Akad Wiss 136(10)

Lai WM, Hou J, Mow VC (1991) A triphasic theory for the swelling and deformation behaviors of articular cartilage. J Biomech Eng 113(3):245–258

Lang GE, Stewart PS, Vella D, Waters SL, Goriely A (2014) Is the Donnan effect sufficient to explain swelling in brain tissue slices? J R Soc Interface 11(96):20140,123

Lemon G, King JR, Byrne HM, Jensen OE, Shakesheff KM (2006) Mathematical modelling of engineered tissue growth using a multiphase porous flow mixture theory. J Math Biol 52(5):571–594

Lu X, Mow V (2008) Biomechanics of articular cartilage and determination of material properties. Med Sci Sports Exerc 40(2):193–199. https://doi.org/10.1249/mss.0b013e31815cb1fc

MacMinn CW, Dufresne ER, Wettlaufer JS (2016) Large deformations of a soft porous material. Phys. Rev. Appl. 5(4):044,020

Manzano S, Armengol M, Price AJ, Hulley PA, Gill HS, Doblaré M, Doweidar MH (2016) Inhomogeneous response of articular cartilage: a three-dimensional multiphasic heterogeneous study. PLoS One 11(6):e0157,967

Manzano S, Manzano R, Doblaré M, Doweidar MH (2015) Altered swelling and ion fluxes in articular cartilage as a biomarker in osteoarthritis and joint immobilization: a computational analysis. J R Soc Interface 12(102):20141,090

Mow V, Kuei S, Lai W, Armstrong C (1980) Biphasic creep and stress relaxation of articular cartilage in compression: theory and experiments. J Biomech Eng 102(1):73–84

Mow V, Kwan M, Lai W, Holmes M (1986) A finite deformation theory for nonlinearly permeable soft hydrated biological tissues. In: Schmid-Schönbein GW, Woo SL, Zweifach BW (eds) Frontiers in biomechanics. Springer, New York, pp 153–179

Mow VC, Mansour JM (1977) The nonlinear interaction between cartilage deformation and interstitial fluid flow. J Biomech 10(1):31–39

Murakami T, Yarimitsu S, Nakashima K, Sakai N, Yamaguchi T, Sawae Y, Suzuki A (2015) Biphasic and boundary lubrication mechanisms in artificial hydrogel cartilage: a review. Proc Inst Mech Eng Part H J Eng Med 229(12, SI):864–878

Pierce D, Ricken T, Holzapfel G (2013) A hyperelastic biphasic fibre-reinforced model of articular cartilage considering distributed collagen fibre orientations: continuum basis, computational aspects and applications. Comput Methods Biomech Biomed Eng 16(12):1344–1361

Raphael B, Khalil T, Workman VL, Smith A, Brown CP, Streuli C, Saiani A, Domingos M (2017) 3D cell bioprinting of self-assembling peptide-based hydrogels. Mater Lett 190:103–106

Rossetti L, Kuntz L, Kunold E, Schock J, Müller K, Grabmayr H, Stolberg-Stolberg J, Pfeiffer F, Sieber S, Burgkart R et al (2017) The microstructure and micromechanics of the tendon-bone insertion. Nat Mater 16(6):664

Soltz MA, Ateshian GA (1998) Experimental verification and theoretical prediction of cartilage interstitial fluid pressurization at an impermeable contact interface in confined compression. J Biomech 31(10):927–934

Wilson W, Huyghe J, Van Donkelaar C (2006) A composition-based cartilage model for the assessment of compositional changes during cartilage damage and adaptation. Osteoarthr Cartil 14(6):554–560

Wilson W, Huyghe J, Van Donkelaar C (2007) Depth-dependent compressive equilibrium properties of articular cartilage explained by its composition. Biomech Model Mechanobiol 6(1–2):43–53

Wilson W, Van Donkelaar C, Huyghe J (2005) A comparison between mechano-electrochemical and biphasic swelling theories for soft hydrated tissues. J Biomech Eng 127(1):158–165

Wilson W, Van Donkelaar C, Van Rietbergen B, Huiskes R (2005) A fibril-reinforced poroviscoelastic swelling model for articular cartilage. J Biomech 38(6):1195–1204